

Geophysical evidence for cyclic sediment deposition on the southern slope of Qiongdongnan Basin, South China Sea

Qi-Liang Sun · Shi-Guo Wu · Thomas Lüdmann · Bin Wang · Tao-Tao Yang

Received: 20 December 2010 / Accepted: 11 March 2011 / Published online: 26 March 2011
© Springer Science+Business Media B.V. 2011

Abstract Gravity flow deposits form a significant component of the stratigraphic record in ancient and modern deep-water basins worldwide. Analyses of high-resolution 3D seismic reflection data in a predominantly slope setting, the southern slope of Qiongdongnan Basin, South China Sea, reveal the extensive presence of gravity flow depositional elements in the Late Pliocene–Quaternary strata. Three key elements were observed: (1) mass transport deposits (MTDs) including slumps and debris flows, (2) turbidity current deposits including distributary channel complexes, leveed channel complexes and avulsion channel complexes, and (3) deep-water drapes (highstand condensed sections). Each depositional element displays a unique seismic expression and internal structures in seismic profiles and attribute maps. Based on seismic characteristics, the studied succession is subdivided into six units in which three depositional cycles are identified. Each cycle exhibits MTDs (slump or debris) at the base, overlain by turbidities or a deep-water drape. The genesis of these

cycles is mainly controlled by frequent sea-level fluctuations and high sedimentation rates in the Late Pliocene–Quaternary. Moreover, tectonics, differential subsidence, and paleo-seafloor morphology may have also contributed to their formation processes. The present study is aimed to a better understanding of deep-water depositional systems, and to a successful hydrocarbon exploration and engineering-risk assessment.

Keywords Deep-water sedimentation · Cyclic deposition · Mass transport deposits · Turbidite · Sea level change · Qiongdongnan Basin

Introduction

The understanding of deep-water depositional systems has advanced significantly in recent years (Posamentier and Kolla 2003). As exploration has focused on deep-water areas, more and more multi-channel high resolution 2D and 3D seismic data were acquired in deep-water settings (e.g., Beaubouef and Friedmann 2000; Posamentier et al. 2000; Posamentier and Kolla 2003; Yuan et al. 2009). The 3D seismic data afford an excellent view of the deep-water depositional environment, in some instances with vertical resolution down to 2–3 m (Posamentier and Kolla 2003). Gravity-induced across-slope sedimentation processes, such as slides, slumps, debris flows, and turbidity currents, are important and predominant on continental slope domains (Yuan et al. 2009). Through compiling from Dott (1963), Nardin et al. (1979), Posamentier and Kolla (2003), Moscardelli et al. (2006), Moscardelli and Wood (2007) and Bull et al. (2009), the terminologies used here and their seismic reflection characteristics are as follows: (1) slide is defined as shear failure along discrete shear planes without

Q.-L. Sun (✉) · S.-G. Wu
Key Laboratory of Marine Geology and Environment,
Institute of Oceanology, Chinese Academy of Sciences,
Qingdao 266071, China
e-mail: sunqiliang@qdio.ac.cn

Q.-L. Sun
Graduate University of Chinese Academy of Sciences,
Beijing 100049, China

T. Lüdmann
Centre of Marine and Atmospheric Sciences,
University of Hamburg, Hamburg, Germany

B. Wang · T.-T. Yang
PetroChina Hangzhou Institute of Geology,
Hangzhou 310023, China

internal deformation or rotation and high-amplitude, continuous reflections; (2) slump is defined as shear failure accompanied by rotation with complicated internal deformation, and low- and high-amplitude chaotic reflections; (3) debris is defined as shear distributed throughout the sediment mass and low-amplitude, semitransparent chaotic reflections, and its basal erosional surface is usually characterized by grooves; (4) turbidity flow is supported by fluid turbulence, and is usually characterized by parallel moderate- to high-amplitude reflections with channel structures.

Many authors have documented the repetitive cycles of mass-transport deposits (MTDs; slide, slump, and debris flows deposits) and channel systems including distributary channel complexes (DCC), leveed channel complexes (LCC), and avulsion channel complexes (ACC) in the Gulf of Mexico (e.g., Beaubouef and Friedmann 2000; Posamentier et al. 2000), Amazon Fan (Pirmez et al. 1997; Manley and Flood 1998), Trinidad and Tobago (Brami et al. 2000; Moscardelli et al. 2006), Nigeria, and Indonesia (Posamentier and Kolla 2003) and attributed them to sea-level change. This depositional pattern is important in understanding the depositional system on slope areas, and is also useful for hydrocarbon exploration.

Turbidity current channels, such as central channel (central canyon), and mass transport deposits have been documented in the Qiongdongnan Basin (Lin et al. 2001; Su et al. 2009; Yuan et al. 2009; Wang et al. 2009; Zhu et al. in press). However, the cyclic depositional pattern observed in this study represents a new aspect in deep-water sedimentation of the South China Sea. This study focuses on the characterization of the seismic facies, geometries, and internal structures of the main depositional elements on the southern slope of Qiongdongnan Basin. It encompasses the evaluation of the potential influences of sea-level fluctuations, sedimentation rate, tectonics and palaeo-seafloor morphology on sedimentation types and their depositional architecture.

Geological setting

The Qiongdongnan Basin lies offshore south Hainan Island with an arc-like shape, and trends NE–SW. The basin is located between 108°51'E and 114°41'E, 17°00'N and 18°50'N (Fig. 1). It is a 290 km long and 181 km wide basin with a total extent of 6,000 km² (Sun et al. 2010). Its western border is marked by a strike-slip fault zone continuing into the Yinggehai Basin (Xie et al. 2006; Wu et al. 2009). The study area is situated on the southern slope of the Qiongdongnan Basin in a present water depth of 1,230–1,300 m, with a seafloor topography dipping NE (Fig. 1).

The Qiongdongnan Basin is a Tertiary basin formed by lithospheric stretching during the Paleogene, followed

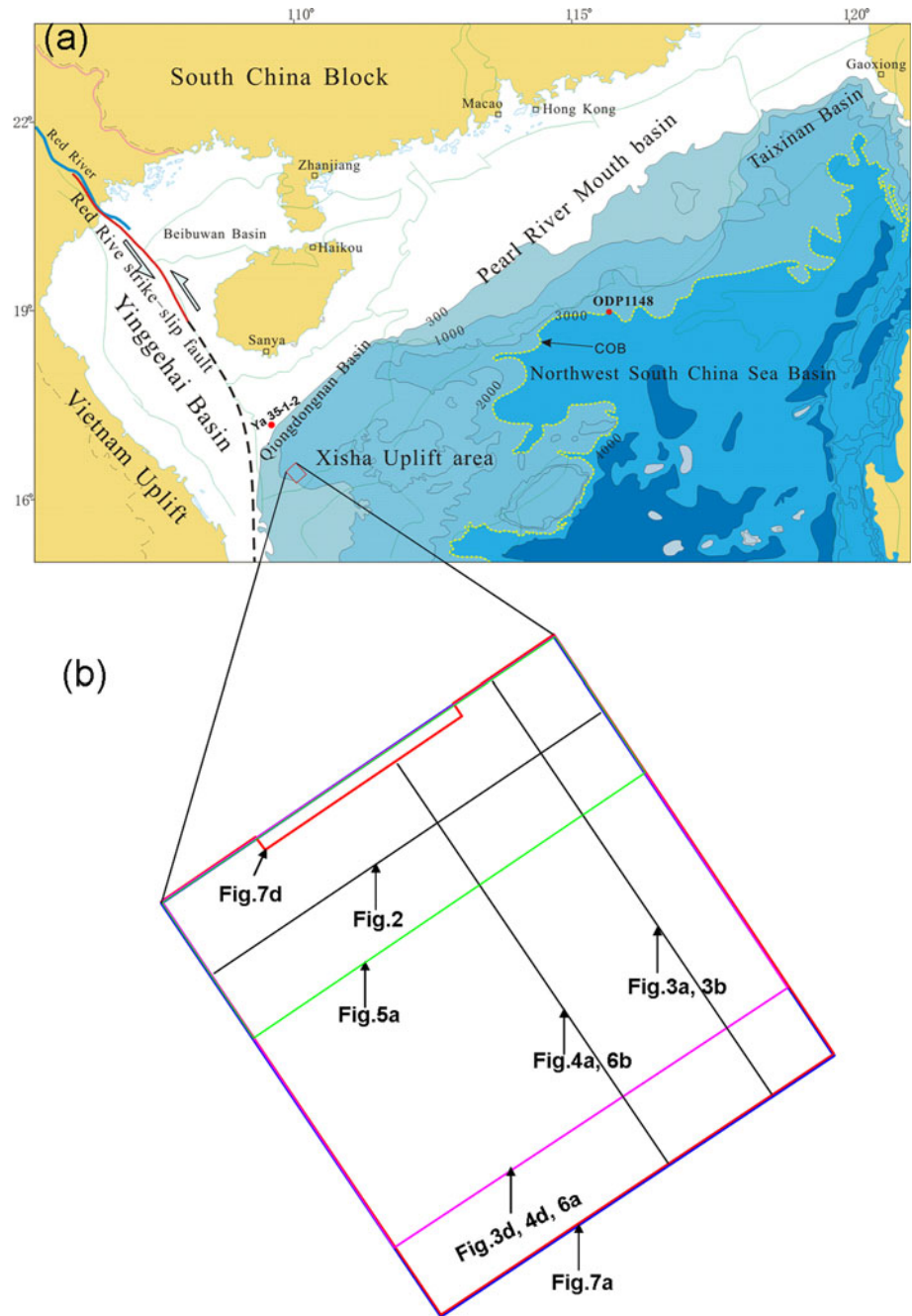
by thermal subsidence since the Miocene (Zhou et al. 1995; Xie et al. 2006). Its sedimentary fill is composed of 2 mega-sequences spanning the rifting period (53.5–23.3 Ma) and post-rifting period (23.3 Ma to Quaternary; Wu et al. 2009), respectively. The depositional environment in the study area was initially transformed from lacustrine to marine conditions and later from neritic to bathyal, starting in Eocene times and continuing to the present (Xie et al. 2006). During the Cenozoic, two main sources provided sediment, namely the South China Block from Oligocene to Miocene and the Vietnam Uplift from Miocene to recent times (Yao et al. 2008; Yuan et al. 2009). Tectonic movements ceased in the post-rifting period (Zhou et al. 1995; Sun et al. 2003). However, a polygonal fault system is well developed in the Mid-Late Miocene succession (Sun et al. 2009, 2010). A turbidity current channel system developed in the study area in the Pleistocene (Yuan et al. 2009). The deposition rate gradually increased since the Miocene time, up to 0.7 mm/year in the Quaternary (Sun et al. 2009). The Red River strike-slip fault, which is one of the major tectonic lineaments in Southeast Asia and is the western boundary of Qiongdongnan Basin, was active as a left-lateral strike-slip fault from Eocene to Miocene; however, it changed its direction of movement and became right-lateral after 5.5 Ma (Morley 2002). Subsequently, the Qiongdongnan Basin was undergoing rapid subsidence (Zhang and Hao 1997).

Data and methods

The primary source of data for this study comprises an industrially acquired 3D reflection seismic dataset. It was acquired by China National Petroleum Corporation (Sun et al. 2010) and covers about 2,800 km², with a CDP (common depth point) interval of 12.5 m and line spacing of 25 m. The data were loaded into work stations and interpreted with the Geoframe software of Schlumberger. The dominant frequency of the data is approximately 60 Hz for the interpreted intervals. We applied an average seismic velocity of 1,700 ms⁻¹ to calculate the resolution in the area of interest, giving a maximum vertical resolution of ca. 7 m and horizontal resolutions of ca. 10 m, respectively.

Horizon-time structure maps were generated from identified and interpreted horizons. Additionally, dip and coherency attribute cubes were extracted from the 3D data. The coherency cube is based on comparison of waveforms across adjacent traces, and gives apparent continuity to discontinuous features, such as faults, edges, and channels (Hart 1999). Dip and coherency cubes are useful for enhancing the appearance of laterally continuous geological features that may otherwise be overlooked (Dalley et al. 1989), such as channels and grooves in the study area, and

Fig. 1 **a** Sketch of the northern South China Sea (modified after Schimanski and Statteger 2005; Yuan et al. 2009); **b** expanded map of the study area on the slope of the Qiongdongnan Basin



avoiding interpretation bias (Bull et al. 2009). Through utilizing a combination of time-structure maps, vertical seismic sections, cube attributes and amplitude attributes, the identification of channels, grooves, folds and thrusts were significantly improved.

Three-dimensional seismic observations and interpretation

Based on the three-dimensional seismic reflection characteristics and internal structures, the interpreted succession

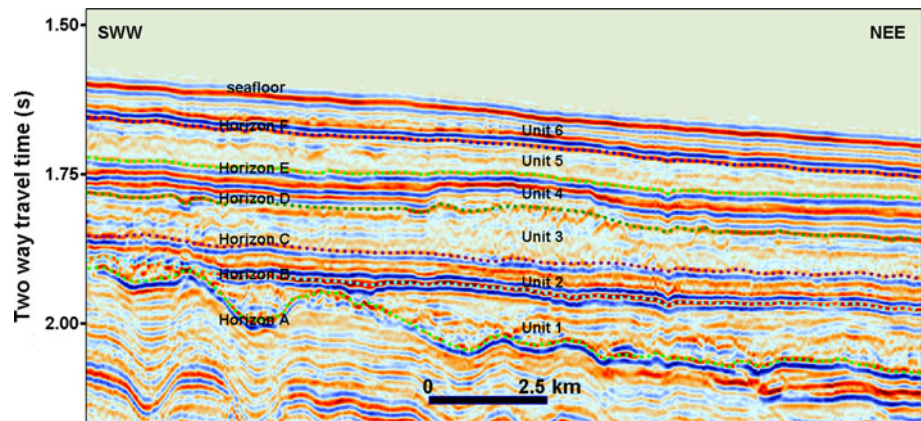
is subdivided into six units (Units 1–6) by mapping seven surfaces throughout the cube, namely Horizons A–F and the seafloor from base to top (Fig. 2).

Unit 1

Observation

Unit 1 marks the base of the interpreted succession, and is bounded by Horizon A and B at its base and top, respectively (Fig. 2). Horizon A is a high-amplitude non-continuous event, and there are widespread onlap and

Fig. 2 Stratigraphic subdivision of the studied sedimentary slope succession. The succession could be subdivided into six seismic units (*Units 1–6*) bounded at base and top by prominent seismic horizons (*Horizons A–F*) and the seafloor, based on -reflection seismic characteristics and internal structures. For location see Fig. 1b



truncation along it. Unit 1 can be subdivided into two sub-units: Unit 1A and Unit 1B, according to their seismic facies and configuration. Unit 1A represents the lower part of Unit 1, which only developed in the northwestern part of the study area (Fig. 3), and it is characterized by low- to -high amplitude, non-continuous to chaotic seismic reflections. The sediments seem to have been rotated along a basal erosional surface (Horizon A, Fig. 3b). The Unit exhibit faulted areas of extension and compressional zones with folds, and thrusts (Fig. 3c). The trend of the extensional faults is nearly NE–SW (Fig. 3d). In the northwestern part of the study area, Unit 1B forms the upper part of Unit 1, and is characterized by semi-transparent, sub-parallel seismic reflections (Fig. 3a, b). It becomes thinner from northwest to southeast and in places it is missing (Fig. 3a, b, c).

Interpretation

The Horizon A is interpreted as major sequence boundary (the boundary between lower Pliocene and upper Pliocene) on the basis of widespread onlap, truncation and borehole correlation (e.g., Ya 35-1-1 on Fig. 1), and its age is determined to 2.9 Ma (Lu and Zhang 1995; Gong and Li 1997; Xie et al. 2008). The complicated internal structures (folds, thrust and extensional faults) and chaotic seismic reflections indicate Unit 1A is a slump. The extensional area is interpreted as head domain, and the fold and thrust area is interpreted as toe domain (Fig. 3c). Unit 1B is interpreted as debris flow based on is semi-transparent, subparallel seismic reflections.

Unit 2

Observation

Unit 2 is bounded by Horizon B and Horizon C (Fig. 2). Horizon B is a very high-amplitude, continuous seismic

reflection event. The internal configuration of Unit 2 is characterized by moderate-amplitude, continuous seismic reflections. The sediment seems to be slight onlap from north to south (Fig. 4).

Interpretation

Because we could not identify any special structure (e.g., channels, grooves, folds and thrusts) in Unit 2 and along Horizon B, and its homogeneous seismic appearance (nearly constant moderate amplitude, Fig. 2) we interpreted the Unit as hemipelagic–pelagic drape. However, onlap termination in the northern part of Unit 2 may indicate the occurrence of turbidities.

Unit 3

Observation

Unit 3 is characterized by low-amplitude, semi-transparent to transparent, subparallel seismic reflection (Fig. 4a, b). It is separated by Horizon C and D from Unit 2 and 4, respectively. In the northern part of the study area its character changes: sediment thickness increases, seismic facies becomes chaotic and many folds and thrusts appear (Fig. 4). Some grooves develop along Horizon C in the attribute map (Fig. 4d).

Interpretation

The northern part of Unit 3 is interpreted as a slump. The grooves are the representative features of basal mass transport deposits. They imply debris flow processes, where the flow direction is parallel to trend of the grooves (Bull et al. 2009). Together with the semi-transparent to transparent seismic reflection pattern, we interpret the rest of Unit 3 as debris flow deposit.

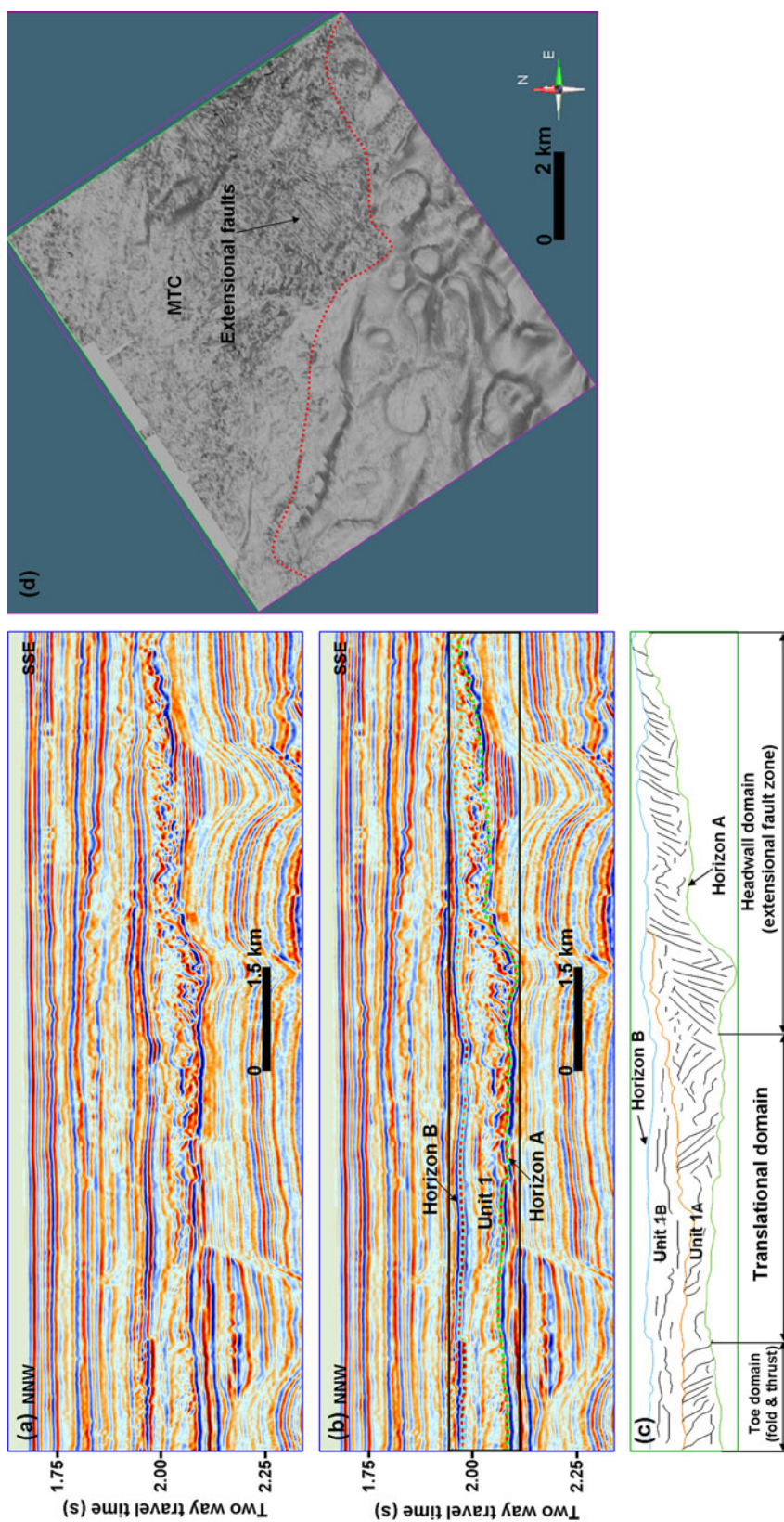


Fig. 3 **a** The un-interpreted version of **(b)**; **b** representative seismic profile for *Unit 1*. The *black square* is the location of **(c)**. For position of *seismic line* see Fig. 1 **b**; **c line** drawing interpretation of *Unit 1*; **d** dip attribute map of *Horizon A*. MTDs (mass transport deposits, the *red dashed line* marks the boundary) and extensive faults are labeled. For location see Fig. 1 **b**

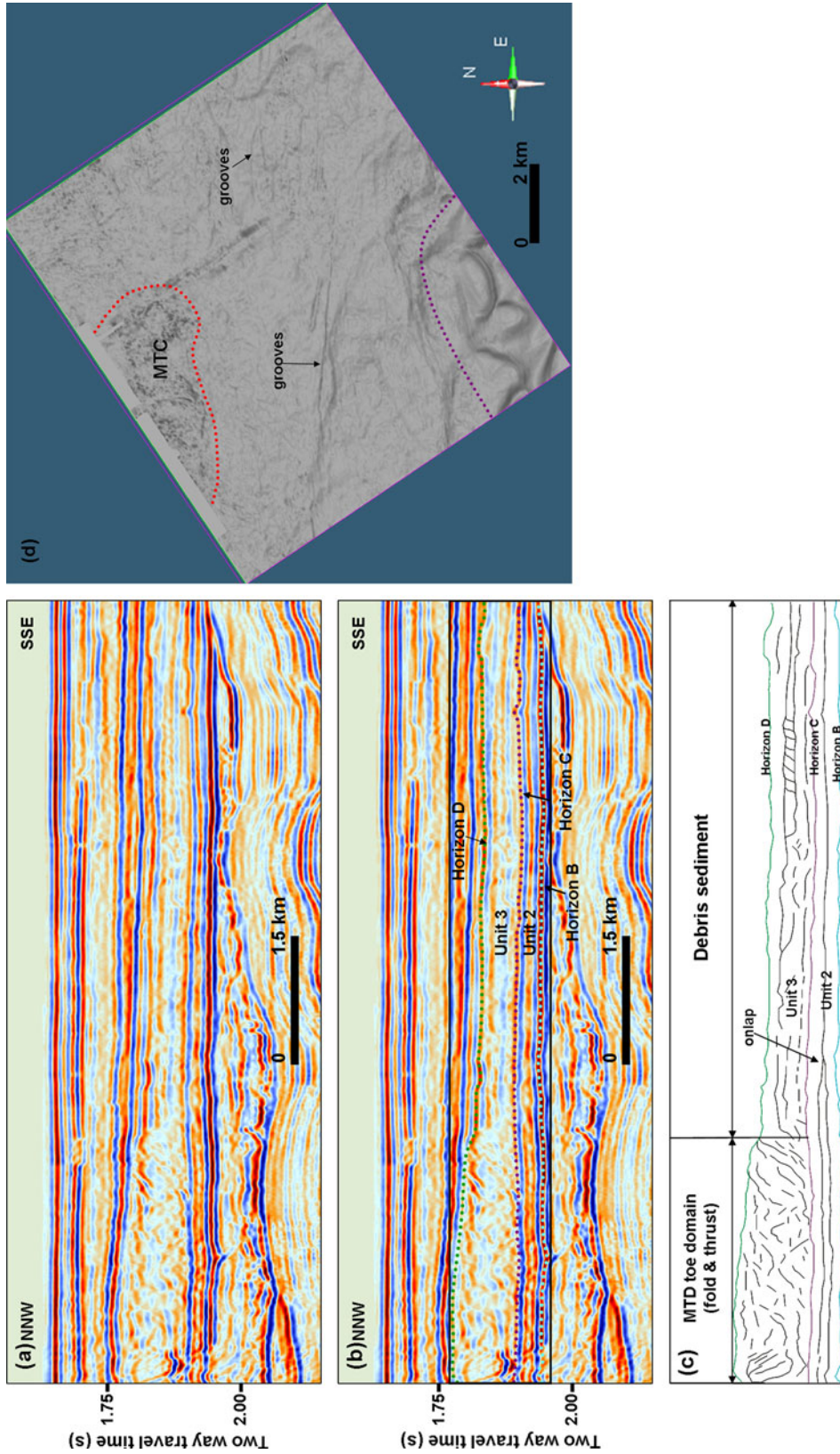


Fig. 4 **a** Un-interpreted version of **(b)**; **b** representative seismic profile of Unit 2 and Unit 3. The black square is the location of **(c)**. For location see Fig. 1**b**; **c** line drawing interpretation of Unit 2 and Unit 3; **d** dip attribute map of Horizon C. MTDs (mass transport deposits), and grooves (the purple dashed line delineates the boundary) are labeled. For location see Fig. 1**b**

Unit 4

Observation

Unit 4 is characterized by predominant high-amplitude, continuous seismic reflections. There are several leveed channels identified in the seismic profiles and dip attribute maps within Unit 4 (Fig. 5). The leveed channels are meandering, and they are 120–350 m wide and trend nearly W to E (Fig. 5b, c). The base of the leveed channels exhibits high amplitude reflection.

Interpretation

The Unit 4 is interpreted as turbidity flow deposits, according to the high-amplitude, continuous reflections and meandering structure in the attribute map. The high amplitude reflection at the base of leveed channels indicates coarse-grained sediments at their base.

Unit 5

Observation

Unit 5 has semi transparent to transparent or chaotic seismic reflections (Fig. 6b, c). Horizon E is a low- to moderate-amplitude, continuous seismic event, with many grooves developed on it (Fig. 6a, b, c). These grooves are long (in some instances longer than 15 km) and linear in plan view. They tend to diverge from SW to NE and E (Fig. 6a). These erosional scours, in some instances more than 10 m deep and over 200 m wide, characterize the base of these semi-transparent to transparent or chaotic deposits. The thickness of Unit 5 is variable, and decreases from SW to NE; giving the Unit an external wedge-shaped geometry (Fig. 6d, e).

Interpretation

A distinctive attribute of debris flow deposits, regardless of whatever their geometries are, is the pattern of grooves that commonly characterizes the basal surface upon which they are deposited (Posamentier and Kolla 2003; Posamentier and Walker 2006). Therefore, the semi-transparent to transparent seismic reflection characteristics and long linear grooves indicate Unit 5 is a typical debris flow deposit.

Unit 6

Observation

Unit 6 is dominated by a moderate- to high-amplitude, parallel and continuous seismic reflection pattern. However, in places additional reflection patterns occur. The first one is a

low-amplitude, V- or W-shaped pattern, whereby the flanks are usually higher than the center (Fig. 7b, c). These seismic reflection features are highly sinuous in plan view (Fig. 7a, marked LC). The incised base of this seismic pattern usually penetrates into Unit 5 and in some instances it reaches its base (Fig. 7b, c). This seismic pattern usually has a narrow base and becomes wider upwards (Fig. 7b, c). The second reflection pattern is a low-amplitude interval embedded into the high amplitude Unit 6. They form small V- or W-shaped incisions (Fig. 7a, b, c, marked DC). In the dip attribute map, the DC is a distributary at the end of LC, and many low-sinuosity depositional bodies diverge downslope (Fig. 7b, c, nearly from W to E and NE). There is third but minor pattern of low-sinuosity in plan view (Fig. 7a, marked AC), it is usually related to LC. It is normally U-shaped in the seismic image; however, its amplitude is generally higher than that of the other two patterns (Fig. 7b, c). The thickness of Unit 6 is homogeneous, except where the turbidity current channels (especially the LCC) occur. The DCC and ACC developed in a limited time interval, ceasing below the modern seafloor. However, the first pattern (LCC) continues to develop until the ocean bottom (Fig. 7d). But its sinuosity is lower, becoming linear basinward with a SW to NE trend (Fig. 7d).

Interpretation

According to the seismic reflection profiles and plan view attribute maps, three channel complexes, LCC (the first seismic-reflection pattern), DCC (the second seismic-reflection pattern) and ACC (the third seismic-reflection pattern), are identified. The LCC has high sinuosity and a leveed structure (Fig. 7a, b, c); the DCC consist of low-sinuosity depositional bodies with a fan-like distribution (Fig. 7a). The ACC usually are considered to be caused by relatively infrequent, large-volume, high-velocity flows (e.g., Pirmez et al. 1997), and the degree of channel instability versus peak-flow volumes decides where an avulsion would occur (Kolla 2007). The avulsion node usually occurs on the outside of a meander bend (Fig. 7a, marked AC₁). This location favors the probability of an avulsion occurring due to flow stripping, but may also represent the zone of highest channel instability (Armitage 2009). The dominant channel infill is fine-grained sediments deduced from the low-amplitude seismic facies (Fig. 7b, c), and only the ACC may be infilled by coarse-grained material (high-amplitude seismic reflections).

Discussions

Vertical stacking patterns

Three primary depositional systems—mass transport deposits (MTDs), turbidity flow deposits, and deep-water

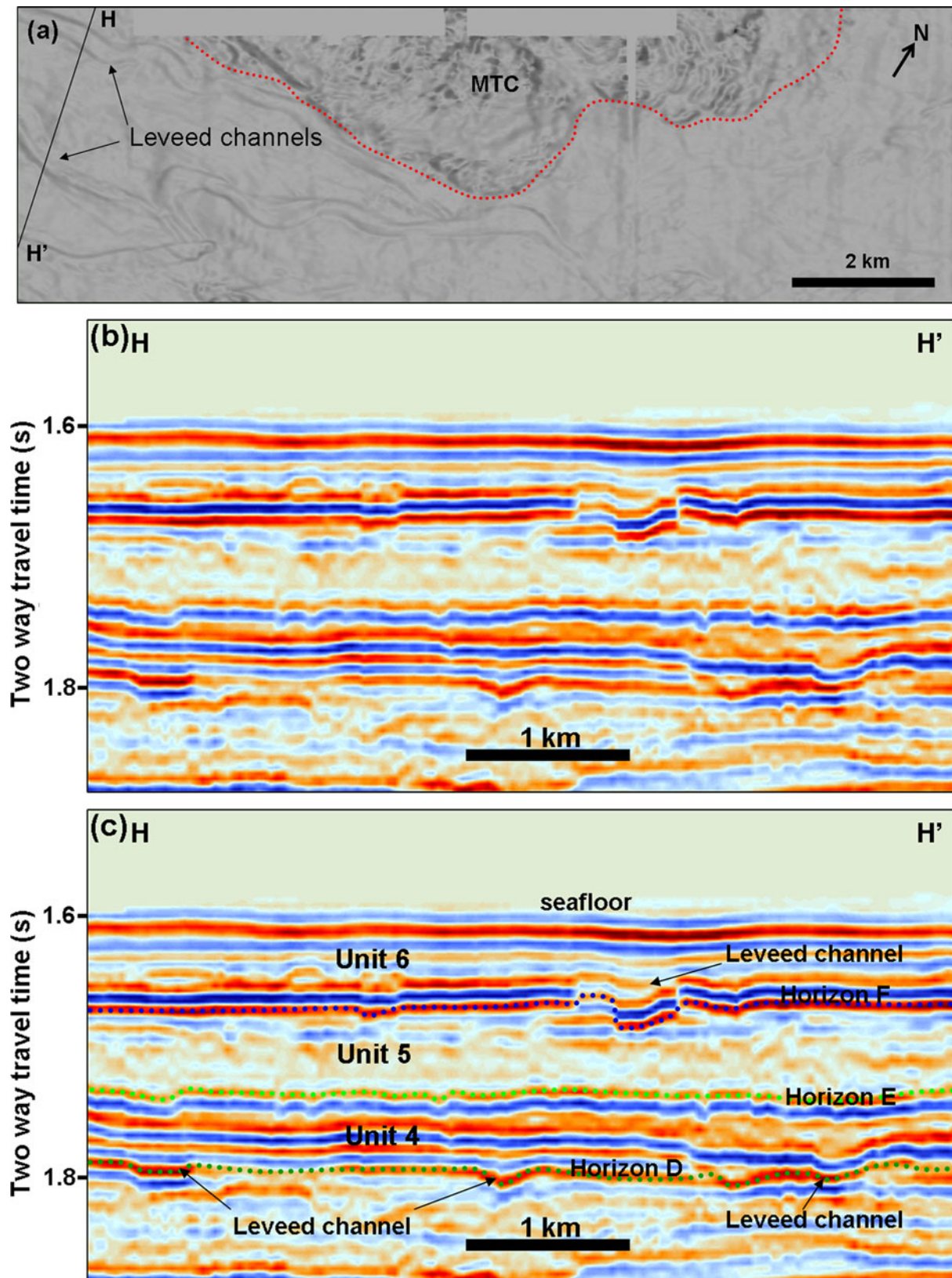


Fig. 5 a Dip attribute map of Horizon D, with some identified leveed channels. For location see Fig. 1b; b un-interpreted version of (c); c a representative *seismic* profile shows the leveed channels within Unit 4

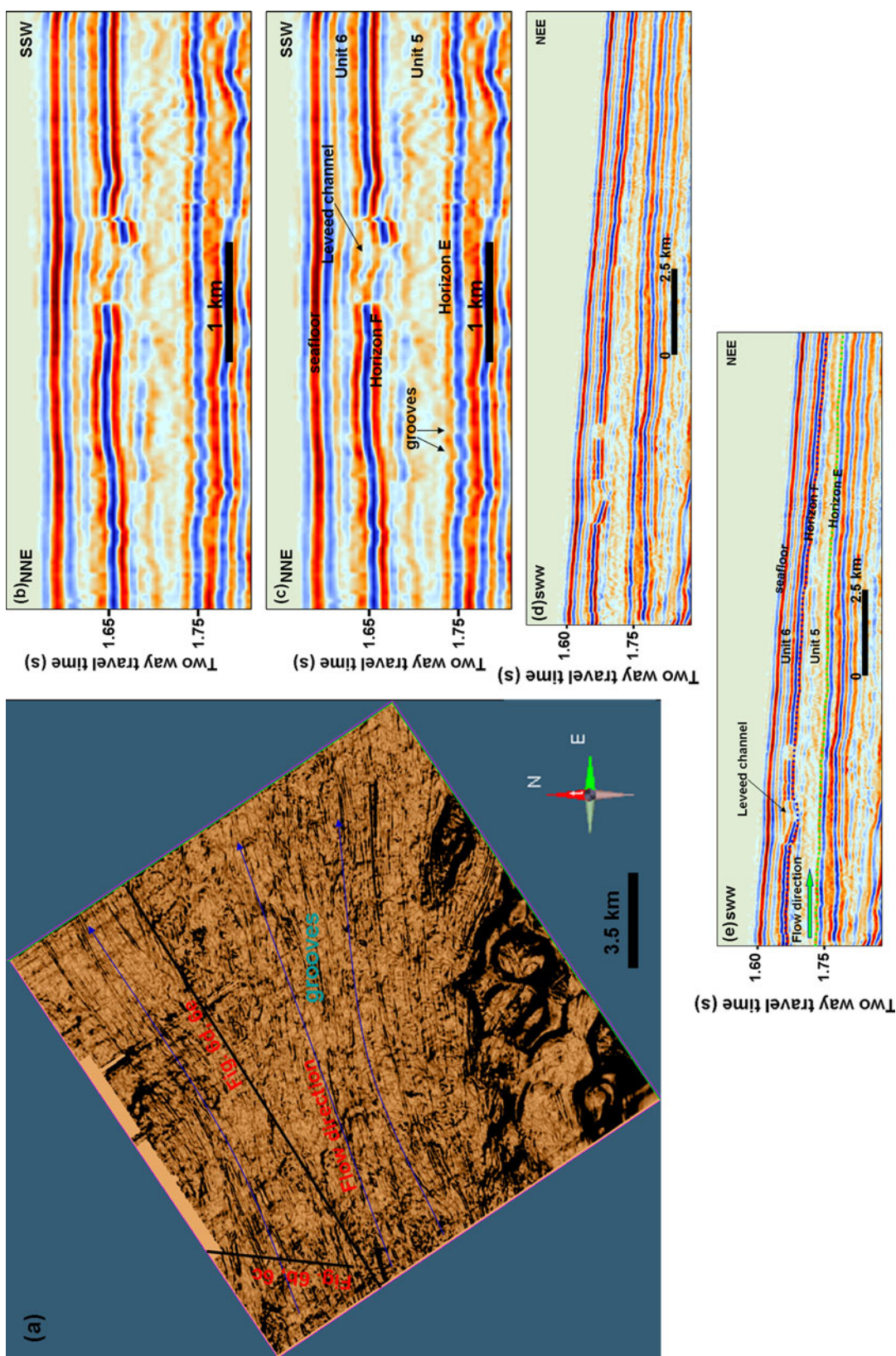


Fig. 6 **a** Dip attribute map at the base of Unit 5 (Horizon E) illustrating long, continuous, linear *grooves*, which show down-slope divergence in map view. For location see Fig. 1b; **b** uninterpreted version of **(c)**; **c** seismic profile across Unit 5. Erosional scours at the base of this unit are locally greater than 10 m deep and 200 m wide; **d** uninterpreted version of **(e)**; **e** seismic profile along *grooves*, which shows that the *thickness* of Unit 5 decreases down-slope

Fig. 7 **a** Dip attribute map at the base of Unit 6 (*Horizon F*) illustrating leveed channels (*LC*, between *red dashed lines*), low-sinuosity distributary-channels (between *blue dashed lines*), and avulsion channels (*AC*). For location see Fig. 1b; **b** the un-interpreted version of (c); **c** a representative seismic profile showing the reflection characteristics of leveed channels, distributary channels, and avulsion channels; **d** time structure map of the seafloor which shows the leveed channel well-developed at the modern seafloor. For location see Fig. 1b

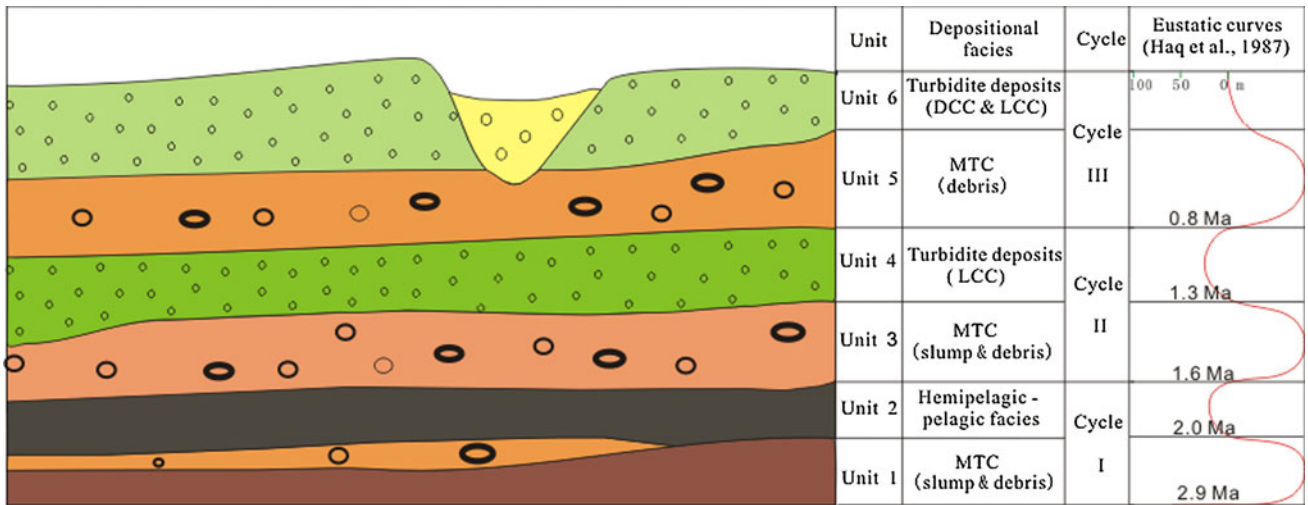
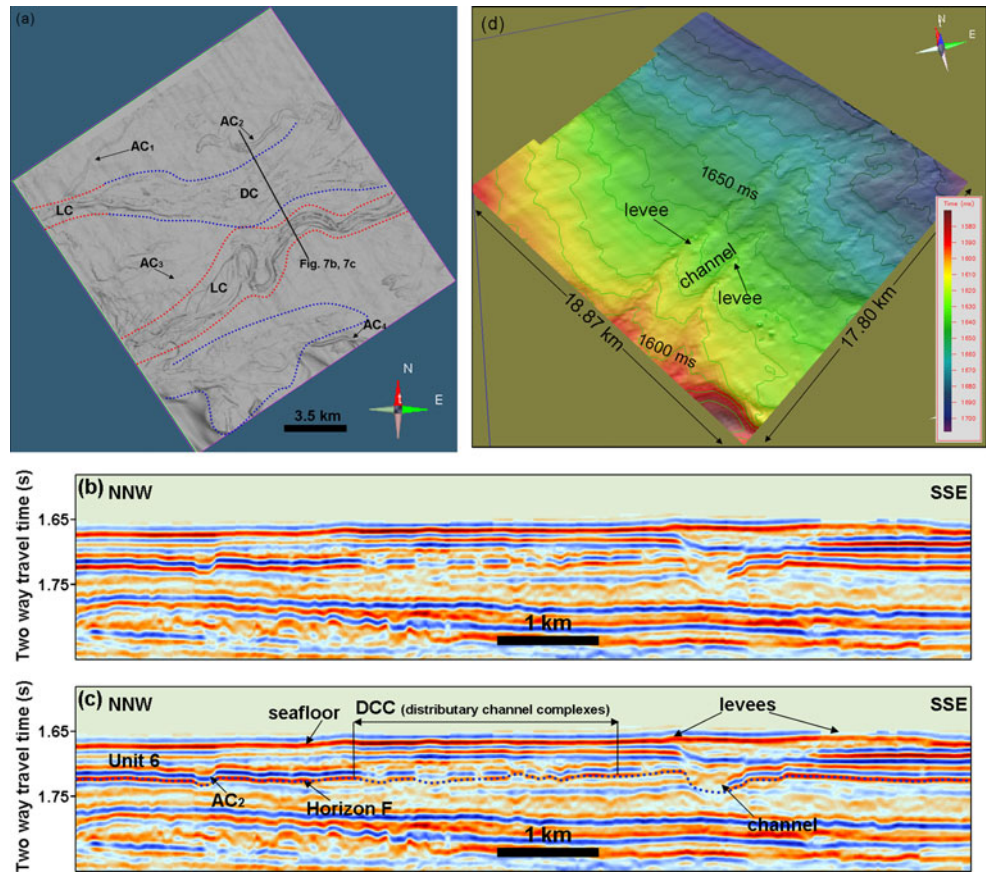


Fig. 8 The vertical depositional stacking pattern in the study area. For details see text

drapes—are identified from the youngest strata on the southern slope of Qiongdongnan Basin, according to the three-dimensional reflection seismic characteristics and internal structures. Two types of MTDs, slump and debris, are developed in the study area, based on the classification by Nardin et al. (1979) and Moscardelli et al. (2006). The slump occurred in two units, Unit 1A and the northern part

of Unit 3. Unit 1A is a small-scale but well developed slump. However, the scale of the slump within Unit 3 is undefined because it extends out of the data, and only the toe domain could be identified (Fig. 4).

Three units (Unit 1B, Unit 3 and Unit 5) are composed of debris-flow deposits. However, the degree of groove development is variable, from well-developed in Unit 5 to

poorly-developed in Unit 3. This variability can be attributed either to differences in sediment caliber and the size of indurated blocks within the respective flows or differences in the degree of induration of the substrate across which the flows travel (Posamentier and Kolla 2003). The common divergence of grooves down-system and the thickness variability from SWW to NEE suggest divergent flow vectors in an unconfined setting and a flow direction from SWW to NEE.

Unit 4 and Unit 6 are predominated by a turbidity current channel system, which includes leveed channel complex (LCC), distributary channel complex (DCC) and avulsion channel complex (ACC). The LCC developed both in Unit 4 and Unit 6, and they are usually of high sinuosity in the attribute maps (Figs. 5a, 7a). The DCC only developed in Unit 6, and it is distinctive with leveed channels in plan view (Fig. 7a). The DCC has a fan-shaped map pattern at the distal end of a feeder channel complex (Fig. 7a). The ACC developed only in Unit 6, and generally with low sinuosity in plan view (Fig. 7a) and steep boundaries in seismic profile (Fig. 7b, c). The avulsion channel usually originated from LC (Fig. 7a, marked AC₁ and AC₃) and DC (Fig. 7a, marked AC₄).

There are no special internal structures in Unit 2, and the seismic-reflection pattern is similar to those of highstand condensed sections (Posamentier and Kolla 2003). Therefore, we identify Unit 2 as hemipelagic–pelagic drape equivalent to a highstand condensed section.

A remarkable characteristic of the stratigraphy and depositional history of the southern slope of Qiongdongnan Basin is the cyclic nature and the repeated stacking patterns that occur. We could identify three cycles in the study area. Mass transport deposits (slump or debris-flow deposits) are found at the base of each cycle and are interpreted to be usually associated with a sequence boundary. These mass transport deposits are commonly overlain by interpreted turbidite successions or a hemipelagic–pelagic drape. For Cycle I, the slump deposits lie at the base and are overlain by debris-flow deposits within Unit 1, finally covered by a deep-water drape (Unit 2). In Cycle II, the slump laterally grade into debris-flow deposits within Unit 3, and then they are overlain by turbidites of Unit 4, which is mainly composed of leveed channel complexes (LCC). In Cycle III, the turbidites (including LCC, DCC, and ACC) of Unit 6 directly overlie the debris-flow deposits of Unit 5 (Fig. 8).

Possible controlling factors

Many factors can control deep-water depositional style and associated features, such as sea-level fluctuation, sediment supply, seafloor topography, tectonics, bottom-current activity, sand-to-mud ratio, steep slope, etc. (Pirmez et al.

1997; Badalini et al. 2000; Beaubouef and Friedmann 2000; Brami et al. 2000; Posamentier and Kolla 2003; Wynn et al. 2007; Armitage et al. 2009). However, the vertical stacking pattern in the study area is slightly different from the characteristics concluded by Posamentier and Kolla (2003). Turbidity flow deposits often develop in highstand system tracts, similar to what Carvajal and Steel (2006) documented. Four factors, as follows, may control this vertical stacking pattern.

(1) *Sea-level fluctuation.* Sea-level change plays an important role in controlling deep-water depositional style (Pirmez et al. 1997; Hernández-Molina et al. 2002; Posamentier and Kolla 2003). Sea-level fluctuations were frequent in Quaternary time (Haq et al. 1987), and the largest sea-level drop was about 150 m in this period (Aharon and Chappell 1986). Horizon A marks the boundary between the upper Pliocene and the lower Pliocene, according to the stratigraphy derived from wells in the northern Qiongdongnan Basin (sequence boundary S27 in Gong and Li 1997 and Xie et al. 2008; Hao et al. 2000), and it is comparable to the sequence boundary at 2.9 Ma, documented by Haq et al. (1987). Horizon C separates the Pliocene from the Quaternary (1.6 Ma, sequence boundary S20 in Lu and Zhang 1995 and Gong and Li 1997; Hao et al. 2000). The turbidites in the study area determined by Yuan et al. (2009) are equivalent to Cycle III. They proposed that the turbidites formed during the Mid-Pleistocene Revolution (MPR, 0.9–0.92 Ma) which is very close to the last significant sea-level drop (at 0.8 Ma) documented by Haq et al. (1987). Therefore, the three depositional cycles are apparently associated with the last three cycles of main sea-level fluctuation since 2.9 Ma proposed by Haq et al. (1987). Because of insufficient well data, we cannot go further. However, based on the previous sequence stratigraphy studies (Lu and Zhang 1995; Gong and Li 1997; Xie et al. 2008), the vertical depositional patterns and comparison with other similar case studies (e.g., Gulf of Mexico, Amazon Fan, and Trinidad and Tobago), the influence of sea-level fluctuation on cyclic deposition in the study area is believable.

(2) *Tectonic reactivation and differential subsidence.* The study area has been in its post-rifting stage since Miocene time (15.5 Ma; Xie et al. 2006), and the tectonic movements ceased in the study area after that (Zhou et al. 1995; Xie et al. 2006). However, the Red River strike-slip fault in the western boundary of the study area reactivated during the Quaternary (Schimanski and Statterger 2005). The dextral slip rate is estimated to be 1–5 mm/yr, according to measurements of the onshore Red River strike-slip fault (Allen et al. 1984). The reactivation of Red River strike-slip fault caused frequent seismicity which has been documented in China (Zhang et al. 1993), Vietnam (Tsai et al. 1999) and, the Qiongdongnan and Yinggehai

basins (Wei and Chung 1995). Tectonic reactivation and related seismicity can cause slope instabilities by seismic shaking, changing pore pressure and creating zones of weakness.

The Qiongdongnan Basin has experienced rapid subsidence since 5.5 Ma (Zhang and Hao 1997). We can also deduce this from the thick Quaternary sediments in the central subsidence belt which is just north of the study area (Xie et al. 2006). Moreover, the northern Vietnam shelf is uplifting in Holocene time, caused by the Red River strike-slip fault movement (Schimanski and Stattegger 2005). Therefore, the rapid relative subsidence in the central subsidence belt which is just north of the study area, and the relative uplift of the Vietnam shelf which is just southwest of the study area will steepen the slope. The steep slope and the reactivated strike-slip fault may have triggered slope instability and slope failure, leading to the generation of slumps, debris flows, and turbidity current flows.

(3) *A high sedimentation rate.* The build-up of excess pore pressure in fine-grained sediments as a result of rapid sedimentation is a potentially important factor in controlling the instability of continental slopes (Zhu et al. in press). The sedimentation rate increases quickly during the last 3 m.y.; it is 400–800 m/m.y. in the northern Qiongdongnan Basin and Yinggehai Basin (Zhu et al. in press), and 50–100 cm/ky (500–1,000 cm/ky for short periods during the early Holocene) on the central Vietnam shelf (Schimanski and Stattegger 2005) in the western South China Sea. The collision of India with Eurasia and the Himalayas would have caused great erosion and abundant sediment were carried into the South China Sea by small mountain rivers and larger rivers (e.g., Pearl River and Red River) whether sea level is high or low (e.g., Schimanski and Stattegger 2005; Xie et al. 2008; Zhu et al. in press). In addition, this high sedimentation rate is also linked to a climate change. Zhang et al. (2001) suggested that disequilibrium states of frequent and abrupt changes in temperature, precipitation and vegetation are effective in causing erosion, but only after 4–3 Ma, as global climate deteriorated. We infer that this rapid increase in sedimentation rate oversteepens the slope deposits and induces large-scale sediment failures on the upper slope, which, in turn, generated large gravity-controlled mass movements. So to some degree, the high sedimentation rate may be more important than the sea-level fluctuation in controlling the special depositional styles such as the turbidity flow deposits developing in the highstand system tract.

(4) *Paleo-seafloor morphology.* The paleo-seafloor morphology plays a primary role in controlling the general distribution and facies architecture of the overlying sediments (Armitage et al. 2009). It would have influenced the flow direction of the downslope deposits. The slope dips

from SW to NE, so most of the debris flows and turbidity flows (e.g., these in Units 1, 3, 5 and 6) trend from SW to NE (Figs. 5a, 6a, 7a).

Implications

The continental slope is an important and active depositional area. It plays an important role in understanding source-to-sink processes (Sømme et al. 2009), and now many studies, such as those on MTDs, channel systems, etc., are focused on this area (e.g., Manley and Flood 1998; Brama et al. 2000; Moscardelli et al. 2006; Sømme et al. 2009). This study discovered new important depositional cycles using high-resolution 3D seismic data. These depositional cycles should be widespread phenomenon in deep-water margin settings worldwide, and may also be prevalent in ancient slope successions. Therefore, our study provides a valuable contribution to the understanding of depositional processes on slope areas.

Through other studies in the Campos Basin, offshore West Africa, and Gulf of Mexico, researchers (e.g., Pettingill and Weimer 2002; Dailly et al. 2002) found that channels in deep-water areas could be excellent reservoirs. MTDs are prone to being cap rocks (Moscardelli et al. 2006; Armitage et al. 2009), because of their mud-dominated sediments and homogeneous physical properties. Hence, the observed cyclic deposits may be an excellent group for deep-water hydrocarbon accumulation. A few turbidite channels in the study area (e.g., these in Unit 4) are infilled by coarse-grained sediments and fall into the style referred above. However, the low amplitude facies within most of the channels, especially those in Unit 6, indicates that the infill is fine-grained (Fig. 7b, c). Therefore, these channel deposits in our study area are not comparable to those described by many researchers (e.g., Pettingill and Weimer 2002; Dailly et al. 2002; Posamentier and Kolla 2003; Armitage et al. 2009). This implies that in general not all channel deposits serve as good reservoirs. It is indispensable to have a good understanding of the depositional facies and stacking pattern, respectively, to gain a better-informed reservoir model and especially to reduce exploration risk. Moreover, the Qiongdongnan Basin is a petroliferous basin, and the mass transport deposits in the shallow surface must be assessed for pipeline design and drilling plans.

Conclusion

Three main depositional elements, namely MTDs (including slump and debris flow deposits), turbidity flow deposits (including DCC, LCC and ACC), and deep-water drapes

are identified embedded in six units, according to 3D seismic data (both seismic profiles and attribute maps). The slumps usually reveal chaotic seismic reflections and are internally folded and thrust. The debris flow deposits are characterized by transparent to semi-transparent up to chaotic seismic reflection pattern and pronounced grooves at their bases. The unique grooves indicate the flow direction and are commonly divergent down-system. The channel system deposits normally have parallel seismic reflections, but within the channels they are usually transparent and different from the host successions. The DCC, LCC and ACC are fan-like, high-sinuosity, and low-sinuosity, respectively, in attribute maps. The three main depositional elements are cyclic in vertical relationship. Three cycles are defined in the study area. Each cycle contain two units, and usually begins with MTDs (slump and/or debris) at the base, and then followed up by turbidity flow deposits or a deep-water drape. These vertical stacking patterns are mainly controlled by sea-level fluctuation and a high sedimentation rate. Our results show that the three cycles may be comparable to the last three sea-level fluctuations since 2.9 Ma recognized by Haq et al. (1987). Moreover, other factors, such as tectonics, differential subsidence, and paleo-seafloor morphology, etc., maybe also contribute to their formation. We assume that this study provides new insight into the understanding of deep-water depositional systems, and may help by the estimation of exploration and engineering risk.

Acknowledgments We thank China National Petroleum Company for permission to release the seismic data. This work was supported by the CAS Knowledge Innovation Program (KZCX2-YW-229), the National Basic Research Program of China (2009CB219406) and the National Scientific foundation of China (Grant No. 40930845). Dominic A. Armitage, Sun Zhen and an anonymous reviewer are thanked for their constructive and thorough reviews and suggestions which significantly improved the manuscript. We are also grateful to the kindly Editor-in-Chief, Amy E. Draut, for her substantial corrections to the English language and helpful suggestions.

References

- Aharon P, Chappell J (1986) Oxygen isotopes, sea level changes and the temperature history of a coral reef environment in New Guinea over the last 10^5 years. *Palaeogeogr Palaeoclimatol* 56:337–379. doi:10.1016/0031-0182(86)90101-X
- Allen CR, Gillespie AR, Han Y, Sieh KE, Zhang B, Zhu C (1984) Red River and associated faults, Yunnan Province, China: Quaternary geology, slip rates, and seismic hazard. *GSA Bull* 95:686–700. doi:10.1130/0016-7606(1984)95<686:RRAAFY>2.0.CO;2
- Armitage DA (2009) High-resolution architectural evolution of depositional elements in deep-marine slope environments: the Quaternary Niger Delta, Quaternary southwest Grand Banks slope, Canada, and Cretaceous Tres Pasos Formation, Chile. Dissertation, Stanford University, pp 2–38
- Armitage DA, Romans BW, Covault JA, Graham SA (2009) The influence of mass-transport-deposit surface topography on the evolution of turbidite architecture: the Sierra Contreras, Tres Pasos formation (Cretaceous), southern Chile. *J Sediment Res* 79:287–301. doi:10.2110/jsr.2009.035
- Badalini G, Kneller B, Winker CD (2000) Architecture and processes in the late Pleistocene Brazos-Trinity turbidite system, Gulf of Mexico continental slope. In: Weimer P, Slatt RM, Coleman J, Rosen NC, Nelson H, Bouma AH, Styzen MJ, Lawrence DT (eds) Deep-water reservoirs of the world. Gulf Coast Society of the Society of Economic Paleontologists and Mineralogists Foundation, 20th Annual Research Conference, Houston, TX, pp 16–34
- Beaubouef RT, Friedmann SJ (2000) High resolution seismic/sequence stratigraphic framework for the evolution of Pleistocene intra slope basins, western Gulf of Mexico: depositional models and reservoir analogs. In: Weimer P, Slatt RM, Coleman J, Rosen NC, Nelson H, Bouma AH, Styzen MJ, Lawrence DT (eds) Deep-water reservoirs of the world. Gulf Coast Society of the Society of Economic Paleontologists and Mineralogists Foundation, 20th Annual Research Conference, Houston, TX, pp 40–60
- Brami TR, Pirmez C, Archie C, Heeralal S, Holman KL (2000) Late Pleistocene deep-water stratigraphy and depositional processes, offshore Trinidad and Tobago. In: Weimer P, Slatt RM, Coleman J, Rosen NC, Nelson H, Bouma AH, Styzen MJ, Lawrence DT (eds) Deep-water reservoirs of the world. Gulf Coast Society of the Society of Economic Paleontologists and Mineralogists Foundation, 20th Annual Research Conference, Houston, TX, pp 104–115
- Bull S, Cartwright J, Huuse M (2009) A review of kinematic indicators from mass-transport complexes using 3D seismic data. *Mar Pet Geol* 26:1132–1151. doi:10.1016/j.marpetgeo.2008.09.011
- Carvajal CR, Steel RJ (2006) Thick turbidite successions from supply-dominated shelves during sea-level highstand. *Geology* 34:665–668. doi:10.1130/G22505.1
- Dailly P, Lowry P, Goh K, Monson G (2002) Exploration and development of Ceiba Field, Rio Muni Basin, Southern Equatorial Guinea. *Lead Edge* 10:1140–1146. doi:10.1190/1.1523753
- Dalley RM, Gevers ECA, Stampfli GM, Davies DJ, Gastaldi CN, Ruijtenberg PA, Vermeer GJO (1989) Dip and azimuth displays for 3D seismic interpretation. *First Break* 7:86–95
- Dott RH (1963) Dynamics of subaqueous gravity depositional processes. *AAPG Bull* 47:104–128
- Gong ZS, Li ST (1997) Continental margin basin analysis and hydrocarbon accumulation of the northern South China Sea. Science Press, Beijing, pp 193–256
- Hao YC, Chen PF, Wan XQ, Dong JS (2000) Late Tertiary sequence stratigraphy and sea level changes in Yinggehai-Qiongdongnan basin (in Chinese with English abstract). *Geo Science* 14: 237–245
- Haq BU, Hardenbol J, Vail PR (1987) Chronology of fluctuating sea levels since the Triassic. *Science* 235:1156–1167. doi:10.1126/science.235.4793.1156
- Hart BS (1999) Definition of subsurface stratigraphy, structure and rock properties from 3-D seismic data. *Earth-Sci Rev* 47: 189–218. doi:10.1016/S0012-8252(99)00029-X
- Hernández-Molina FJ, Somoza L, Vázquez JT, Lobo F, Fernández-Puga MC, Llave E, Díaz-del Río V (2002) Quaternary stratigraphic stacking patterns on the continental shelves of the southern Iberian Peninsula: their relationship with global climate and palaeoceanographic changes. *Quatern Int* 92:5–23. doi:10.1016/S1040-6182(01)00111-2
- Kolla V (2007) A review of sinuous channel avulsion patterns in some major deep-sea fans and factors controlling them. *Mar Pet Geol* 24:450–469. doi:10.1016/j.marpetgeo.2007.01.004

- Lin CS, Liu JY, Cai SX, Zhang YM, Lü M, Li J (2001) The depositional architecture and development setting of large incised valley and submarine gravity-flow system in Qiongdongnan and Yinggehai basins (in Chinese). *Chinese SCI Bull* 46:69–72
- Lu M, Zhang YZ (1995) Study on depositional systems and sequence stratigraphy in the Yinggehai and Qiongdongnan basins. Research Report of China Offshore Oil Nanhai West Corporation, Zhanjiang
- Manley L, Flood RD (1998) Cyclic sediment deposition within Amazon deep-sea fan. *AAPG Bull* 72:912–925
- Morley CK (2002) A tectonic model for the Tertiary evolution of strike-slip faults and rift basins in SE Asia. *Tectonophysics* 347:189–215. doi:10.1016/S0040-1951(02)00061-6
- Moscardelli L, Wood L (2007) New classification system for mass transport complexes in offshore Trinidad. *Basin Res* 20:73–98. doi:10.1111/j.1365-2117.2007.00340.x
- Moscardelli L, Wood L, Mann P (2006) Mass-transport complexes and associated processes in the offshore area of Trinidad and Venezuela. *AAPG Bull* 90:1059–1088. doi:10.1306/02210605052
- Nardin TR, Hein FJ, Gorsline DS, Edwards BD (1979) A review of mass movement processes, sediment, and acoustic characteristics and contrasts in slope and base-of-slope systems versus canyon-fan-basin floor systems. *Spec Publ Soc Econ Paleontol Mineralog* 27:61–73. doi:10.2110/pec.79.27.0061
- Pettingill HS, Weimer P (2002) World wide deep water exploration and production: past, present, and future. *Lead Edge* 21:371–376. doi:10.1190/1.1471600
- Pirmez C, Hiscott RN, Kronen JK (1997) Sandy turbidite successions at the base of channel-levee systems of the Amazon Fan revealed by FMS logs and cores: unraveling the facies architecture of large submarine fans. In: Flood RD, Piper DJW, Klaus A, Peterson LC (eds). *Proceedings ODP, Scientific results* 155, pp 7–22
- Posamentier HW, Kolla V (2003) Seismic geomorphology and stratigraphy of depositional elements in deep-water settings. *J Sediment Res* 73:367–388. doi:10.1306/111302730367
- Posamentier HW, Walker RG (2006) Deep-water turbidites and submarine fans. In: Posamentier HW, Walker RG (eds) *Facies models revisited*. SEPM Special Publication 84:399–520
- Posamentier HW, Meizarwin Wisman PS, Plawman T (2000) Deep water depositional systems—ultra-deep Makassar Strait, Indonesia. In: Weimer P, Slatt RM, Coleman J, Rosen NC, Nelson H, Bouma AH, Styzen MJ, Lawrence DT (eds) *Deep-water reservoirs of the world*. Gulf Coast Society of the Society of Economic Paleontologists and Mineralogists Foundation, 20th Annual Research Conference, Houston, TX, pp 806–816
- Schimanski A, Statterger K (2005) Deglacial and Holocene evolution of the Vietnam shelf: stratigraphy, sediments and sea-level change. *Mar Geol* 214:365–387. doi:10.1016/j.margeo.2004.11.001
- Sømme TO, Helland-Hansen W, Martinsen OJ, Thurmond JB (2009) Relationships between morphological and sedimentological parameters in source-to-sink systems: a basis for predicting semi-quantitative characteristics in subsurface systems. *Basin Res* 21:361–387. doi:10.1111/j.1365-2117.2009.00397.x
- Su M, Li JL, Jiang T, Tian SS, Zhang C, Xie XN (2009) Morphological features and formation mechanism of central canyon in the Qiongdongnan Basin, northern South China Sea (in Chinese with English abstract). *Marine Geol Quat Geol* 29:85–93. doi:10.3724/SP.J.1140.2009.04085
- Sun Z, Zhou D, Zhong ZH, Zeng ZX, Wu SM (2003) Experimental evidence for the dynamics of the formation of the Yinggehai Basin, NW South China Sea. *Tectonophysics* 372:41–58. doi:10.1016/S0040-195(03)00230-0
- Sun QL, Wu SG, Yao GS, Lv FL (2009) Characteristics and formation mechanism of Polygonal faults in Qiongdongnan Basin, northern South China Sea. *J Earth Sci* 20:180–192. doi:10.1007/s12583-009-0018-z
- Sun QL, Wu SG, Lv FL, Yuan SQ (2010) Polygonal faults and their implications for hydrocarbon reservoirs in the southern Qiongdongnan Basin, South China Sea. *J Asian Earth Sci* 39:470–479. doi:10.1016/j.jseaes.2010.04.002
- Tsai YB, Wu HH, Dinh VT, Trinh VB, Nguyen TY, Phan TKV (1999) Development of a seismic network in Viet Nam to study on seismicity of the Red River fault zone. *J Geol Ser B* 13–14:304–306
- Wang DW, Wu SG, Dong DD, Yao GS, Cao QB (2009) Seismic characteristics of Quaternary mass transport deposits in Qiongdongnan Basin (in Chinese with English abstract). *Marine Geol Quat Geol* 29:69–74. doi:10.3724/SP.J.1140.2009.03069
- Wei BZ, Chung WY (1995) Strike-slip faulting on the northern margin of the South China Sea; evidence from two earthquakes offshore of Hainan Island, China, in December 1969. *Tectonophysics* 241:55–66. doi:10.1016/0040-1951(94)00163-4
- Wu SG, Yuan SQ, Zhang GC, Ma YB, Mi LJ, Xu N (2009) Seismic characteristics of a reef carbonate reservoir and implications for hydrocarbon exploration in deep water of the Qiongdongnan Basin, Northern South China Sea. *Mar Petrol Geol* 26:817–823. doi:10.1016/j.marpetgeo.2008.04.008
- Wynn RB, Cronin BT, Peakall J (2007) Sinuous deep-water channels: genesis, geometry and architecture. *Mar Petrol Geol* 24:341–387. doi:10.1016/j.marpetgeo.2007.06.001
- Xie XN, Mülle RD, Li ST, Gong ZS, Steinberger B (2006) Origin of anomalous subsidence along the Northern South China Sea margin and its relationship to dynamic topography. *Mar Petrol Geol* 23:745–765. doi:10.1016/j.marpetgeo.2006.03.004
- Xie XN, Müller RD, Ren JY, Jiang T, Zhang C (2008) Stratigraphic architecture and evolution of the continental slope system in offshore Hainan, northern South China Sea. *Mar Geol* 247:129–144. doi:10.1016/j.margeo.2007.08.005
- Yao GS, Yuan SQ, Wu SG (2008) The double provenance supply depositional model and its exploration prospect in the deepwater of Qiongdongnan Basin (in Chinese with English abstract). *Petroleum Exploration and Development* 35:679–685
- Yuan SQ, Wu SG, Lüdmann T, Yao GS, Lv FL, Cao F, Wang HR, Li L (2009) Fine-grained Pleistocene deepwater turbidite channel system on the slope of Qiongdongnan Basin, northern South China Sea. *Mar Petrol Geol* 26:1441–1451. doi:10.1016/j.marpetgeo.2009.03.007
- Zhang Q, Hao F (1997) Evolution and petroleum systems of the Ying-Qiong Basin. *Sci China Ser D* 40:553–560. doi:10.1007/BF02877623
- Zhang JG, Wang LM, Xu YJ, Han Y (1993) Analysis of mechanics property of the medium under the deep seismic source environment along the Red River fault (in Chinese with English abstract). *Seismol Geol* 15:131–137
- Zhang PZ, Molnar P, Downs WR (2001) Increased sedimentation rates and grain sizes 2–4 Myr ago due to the influence of climate change on erosion rates. *Nature* 410:891–897. doi:10.1038/35073504
- Zhou D, Ru K, Chen HZ (1995) Kinematics of Cenozoic extension on the South China Sea continental margin and its implications for the tectonic evolution of the region. *Tectonophysics* 251:161–177. doi:10.1016/0040-1951(95)00018-6
- Zhu MZ, Mchargue T, Graham SA, in press, 3-D seismic-reflection characterization of submarine slides on a Pliocene siliciclastic continental slope and its implications for tectonics, sediment supply, and climate change, South China Sea. In: Posamentier HW, Shipp C, Weimer P (eds) *Submarine slope systems*. SEPM Special Publication